The Journal of Chemical Physics

RESEARCH ARTICLE | OCTOBER 07 2022

Structure and dynamics of tail-free discotic liquid crystals: Simulations of fluorinated triphenylene

M. Powers ✉; R. J. Twieg; J. Portman; ... et. al

Check for updates

J. Chem. Phys. 157, 134901 (2022)
https://doi.org/10.1063/5.0106722

View Online Export Citation CrossMark

Articles You May Be Interested In

Structural, electronic, and optical properties of a prototype columnar discotic liquid crystal

J. Chem. Phys. (November 2008)

Electron transport across metal/discotic liquid crystal interfaces

Journal of Applied Physics (March 1998)

Proton NMR study of a discotic columnar mesophase

J. Chem. Phys. (December 1981)

AIP Publishing

Downloaded from http://pubs.aip.org/aip/jcp/article-pdf/doi/10.1063/5.0106722/16552584/134901_1_online.pdf

The Journal of Chemical Physics ARTICLE scitation.org/journal/jcp

Structure and dynamics of tail-free discotic liquid crystals: Simulations of fluorinated triphenylene

Cite as: J. Chem. Phys. 157, 134901 (2022); doi: 10.1063/5.0106722
Submitted: 29 June 2022 • Accepted: 9 September 2022 •
Published Online: 7 October 2022

View Online Export Citation CrossMark

M. Powers,[1,a)] R. J. Twieg,[2] J. Portman,[1] and B. Ellman[1]

AFFILIATIONS

[1] Department of Physics, Kent State University, Kent, Ohio 44242, USA
[2] Department of Chemistry and Biochemistry, Kent State University, Kent, Ohio 44242, USA

[a)] **Author to whom correspondence should be addressed:** mpower16@kent.edu

ABSTRACT

Recently, a large family of at least 14 discotic liquid crystals was discovered that are exceptions to the conventional paradigm that discotic mesogens tend to feature long, flexible tails on their periphery. To understand why these materials are liquid crystals, as well as the structural determinants of discotic phase behavior, we studied a group of closely related small tail-free disk-like molecules, including both mesogenic and non-mesogenic compounds differing only in the position of a single fluorine substituent. The rigidity and structural simplicity of these molecules make them well suited to for study by large, fully all-atom simulations. Using a combination of static and dynamic metrics, we were able to identify several key features of the columnar mesophase and, thereby, conclusively identify a columnar liquid crystalline mesophase present in a subset of our systems. Our simulations feature molecules hopping between columns in the columnar mesophase and distinctive molecular rotations in 60° steps about the columnar axis. The ability to create and characterize columnar mesophases *in silico* provides a potent tool for untangling the structural determinants of liquid crystalline behavior in these and other tail-free discotic liquid crystals.

Published under an exclusive license by AIP Publishing. https://doi.org/10.1063/5.0106722

I. INTRODUCTION

Discotic liquid crystals (DLCs) are a large class of materials consisting of disk-like molecules that exhibit partially ordered liquid crystal states (mesophases). They are most commonly associated with the columnar mesophase in which molecules assemble themselves into long columns, which are arranged to form a two dimensional lattice. Aside from possessing a columnar mesophase, DLCs are also known to form nematic and smectic mesophases,[1–3] though the columnar mesophase is the subject of this work. In the hexagonal columnar mesophase, the columns have a moderate degree of intracolumn molecular order and form a highly ordered hexagonal lattice. They have excited interest, in particular, due to their favorable quasi-one dimensional electronic transport properties.[4,5] The vast majority of discotic molecules with a columnar mesophase share a common structural motif: They have rigid, often highly conjugated cores, surrounded by long flexible tails. The tails serve to reduce intercolumnar interactions as well as to provide a source of entropy, which is thought to stabilize the mesophase.[6] Tails are so ubiquitous that descriptions of DLCs often assume their presence. However, tails are *not* required for a DLC to have a columnar mesophase. A small number of tail-free thermotropic DLCs are known, including small halogenated indenes and pseudoazulenes[7] and a growing family of halogenated triphenylenes.[8] In addition to these thermotropic tail-free DLCs, colloidal suspensions of platelets are known to form a columnar mesophase,[9] and coarse-grained simulations of hard[10–14] and soft core objects[15–19] have also been shown to be able to form a columnar mesophase. From a computational point of view, these small thermotropic tail-free liquid crystals are ideal subjects for molecular dynamics studies as their small rigid structures and lack of entropic tails make them more computationally facile than their long tailed analogs. All-atom simulations of these tail-free molecules can provide detailed information relating the structure of the molecules to properties of their mesophase, as has been done with conventional tailed DLCs.[20–28] At the same time, their small and simple structures have the advantage of increased computational efficiency that makes

Downloaded from http://pubs.aip.org/aip/jcp/article-pdf/doi/10.1063/5.0106722/16552584/134901_1_online.pdf

Published under an exclusive license by AIP Publishing

longer timescales more accessible, which would otherwise require using coarse-grained models or substantial computational resources. The tail-free DLCs benefit from the detail of all-atom simulations and the long timescale dynamics typical of coarse-grained models.

In this work, we focus on a group of tail-free DLCs based on 1,2,3,4-tetrafluorotriphenylene with an additional fluorine substituted at the 5, 6, 7, or 8 position. For convenience, we refer to these based on the position of the substituted fluorine (e.g., F6 for 1,2,3,4,6-pentafluorotriphenylene). These materials have recently been synthesized and two of them (F7 and F8) possess a columnar mesophase.[8] These small tail-free molecules are well suited to atomistic simulations as they have a simple structure consisting of only 30 atoms in highly conjugated, rigid structures. Furthermore, the onset of mesogenic behavior is a result of changing the position of a single fluorine atom. Through the use of all-atom simulations, we are able to study the relationship between the molecular structure and their unusual phase behavior.

Based on experimental results, we would anticipate simulations of F7 and F8 to show mesogenic behavior. We have found mesogenic behavior in our simulations of F6, F7, and F8 *but not* F5. Not only were our simulations of sufficient size and duration to be able to identify dynamic properties, including hopping between columns, but the simple interaction models we used (based on van der Waals and point charge based electrostatic interactions) were sufficient to at least partially discriminate between mesogens and non-mesogens. While alternative force fields may be needed to more completely reproduce and predict the mesophase behavior of these materials, the present models have already given us useful insights.

II. METHODS

A. Molecular structure

The molecular structure and electronic properties of each of the compounds were determined via density functional theory (DFT) calculations. Structures were optimized at the 6-311g** level using the B3LYP functional.[29] Atom-centered partial charges were computed under the same conditions by fitting the electrostatic potential using the Merz-Singh-Kollman (MK) method.[30,31] The optimized structures were kept fixed throughout the simulation. The partial charges and molecular structures are provided in the supplementary material. Intermolecular interactions were limited to electrostatic interactions between the partial charges and van der Waals interactions using Optimized Potentials for Liquid Simulation All-Atom (OPLS-AA)[32] force field parameters. We used a nonpolarizable force field because of the limited polarizability associated with C–F, C–C, and C–H bonds.[33,34] This resulted in a simple and computationally efficient model for intermolecular interactions. Notably, one proposed explanation for the mesogenic behavior of other halogenated tail-free DLCs is that the molecular polarizability plays the role of an "unusual soft part."[7] However, we see mesophase behavior resulting from rigid molecules interacting through nonpolarizable force fields, i.e., completely without soft parts.

The largest geometric difference between the molecules is a pronounced warping of the F5 and F8 molecules due to steric crowding resulting from the fifth fluorine atom interacting with the adjacent perfluorinated or nonfluorinated rings, respectively. This causes the rings to twist out of the molecular plane, resulting in an aspect ratio (thickness/diameter) of ~0.36 (compared to 0.3 for the flat molecules, F6 and F7). This is especially pronounced in F5, where F–F interactions force a larger deviation from the molecular plane. The dihedral angles (defined in Fig. 1) and the root mean squared (rms) displacement of atoms from the molecular plane serve to quantify the degree of molecular distortion. These values, along with calculated dipole moments, are collected in Table I. The molecular warping interferes with the cofacial alignment of neighboring molecules, resulting in more disordered columns. Additionally, it is expected that the warped molecular cores make rotations more difficult as they require a larger free volume in order to rotate.

B. Simulation details

To track the molecular orientations, we define a coordinate system for each molecule inspired by the geometry of the parent compound, 1,2,3,4-tetrafluorotriphenylene. We define the molecular director, $\hat{n}_i$, as being perpendicular to the molecular plane, found by minimizing the average orthogonal distance between atoms and the plane. We define an additional vector, $\hat{f}_i$, for each molecule that extends from the centroid of a molecule, bisects the perfluorinated ring, and is projected onto the molecular plane so that it is perpendicular to $\hat{n}_i$ (as shown in Fig. 1). The sign of the molecular director is fixed such that $\hat{n}_i \times \hat{f}_i$ points toward the monofluorinated ring. This set of definitions makes comparisons between molecules simple as these reference vectors are qualitatively consistent across the simulated molecules.

All of the molecular dynamics simulations were carried out using the Tinker molecular dynamics program.[35] The systems each consisted of 30 columns of 20 molecules each for a total of 600 molecules. We used an NPT ensemble (constant number of

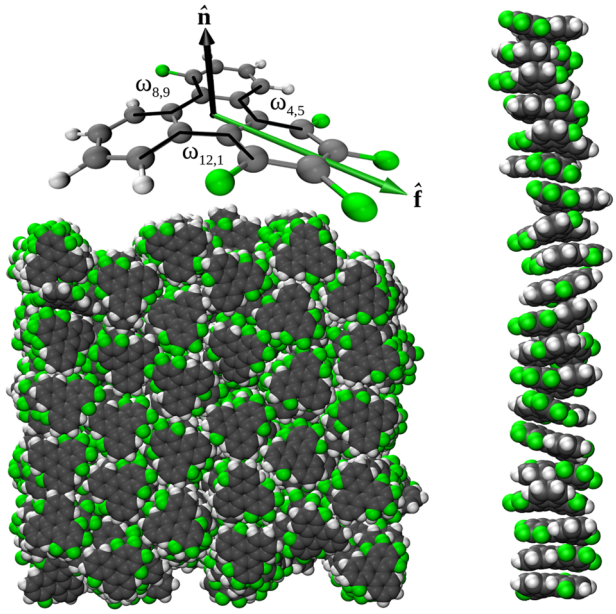

FIG. 1. Illustration of a typical simulated system (F8 in its mesophase), with the bulk system, a typical column, and a molecule shown. The molecule shows the vectors $\hat{n}$ and $\hat{f}$, with the dihedral angles marked (the average dihedral angles are listed in Table I, and the individual angles are included in the supplementary material).

Downloaded from http://pubs.aip.org/aip/jcp/article-pdf/doi/10.1063/5.0106722/16552584/134901_1_online.pdf

Published under an exclusive license by AIP Publishing

TABLE I. Details of the model molecules.

Compound	Dipole moment (D)	rms deviation[a] (Å)	$\langle\|\omega\|\rangle$[b] (deg)	Aspect ratio	Phase sequence[c] (°C)
F5	4.33	0.411	15.1	0.37	K_1 133[d] K_2 152 I 148 K_2
F6	3.53	0.179	7.0	0.30	K 222 I 218 K
F7	2.13	0.175	6.9	0.30	K 193 P 205 I 201 Col_h 198 P 179 K
F8	2.03	0.315	12.2	0.35	K_1 113 K_2 170 Col_h 196 I 194 Col_h 166 K_2 109 K_1

[a]rms deviation measured perpendicular to the molecular plane.
[b]The average dihedral angles. Individual angles, $\omega_{i,j}$, are defined in Fig. 1 and included in the supplementary material.
[c]1,2,3,4,X-pentafluortriphenylene transition sequences. Temperatures and enthalpies obtained from second cycle of DSC at 5 °C/min except where noted. K phases are crystal states, P is a plastic crystal, Col_h is a hexagonal columnar liquid crystal mesophase and I is an isotropic liquid. Additional details on the experimental identification of the phases are forthcoming.[8]
[d]K_1 to K_2 transition temperature reported from first scan at 10 °C/min. Sample remains in the K_2 state throughout subsequent cycles.

molecules, pressure and temperature) at 1.0 atm, with 5 fs steps and atomic coordinates collected every picosecond. The temperature and pressure were controlled using Bussi velocity scaling[36] and a Berendsen barostat,[37] with anisotropic pressure allowing each dimension of the box to be adjusted separately. The lack of tails and use of rigid body dynamics allowed for the somewhat large 5 fs time steps. Van der Waals and electrostatic interactions were cut off at 10 and 15 Å, respectively, with a shifted energy switching tapering scheme used for the electrostatic interactions to avoid impulses stemming from a discontinuity at the cutoff and limit artifacts introduced by the finite interaction range.[35,38] The van der Waals cutoff is easily justified as the interactions between all but nearest neighbors quickly become negligible. The Coulomb interactions are much longer ranged and require a longer cutoff distance and tapering in order to limit undesirable effects on molecular orientations.[39–41] An appropriate cutoff distance was chosen after carrying out limited duration simulations using cutoff distances between 10 and 25 Å and comparing their forces and torques to those generated using a particle Ewald mesh, with 15 Å being selected as it agreed well with the particle Ewald mesh values while being significantly faster. Additionally, a small number of simulations were carried out using a 20 Å electrostatic interaction cutoff, which were found to be in satisfactory agreement with our 15 Å simulations. The 15 Å electrostatic cutoff distance is sufficiently large to include the neighboring columns and is smaller than half the shortest box dimension (which at all times and temperatures is greater than 50 Å).

In the first part of the initialization process, the columns were arranged to form a hexagonal array that packs densely to fill an orthorhombic box with periodic boundary conditions and with the columnar axes aligned with the lab z-axis in order to emulate the structure of a hexagonal columnar mesophase (Fig. 1). This was done by placing molecules into columns separated by a large distance (greater than the interaction cutoff distances), and the columnar lattice was formed by using a series of columnar restraints to drag the columns into position at a temperature of 600 K before rapidly cooling the system to 400 K. These constraints took the form of flat bottom harmonic potential wells applied to each column as a whole, based on columnar restraining potentials used elsewhere.[23] The potential felt by a molecule within the cth column was given by

$$V(\vec{r_{c,i}}) = \begin{cases} 0, & |\vec{r_{c,i}} - \vec{R_c}| \le \delta r, \\ k(|\vec{r_{c,i}} - \vec{R_c}| - \delta r)^2, & |\vec{r_{c,i}} - \vec{R_c}| > \delta r, \end{cases} \quad (1)$$

where $\vec{r_{c,i}}$ is the position in the x–y plane of the ith molecule of the cth column, $\vec{R_c}$ is the center of mass of the cth column, with δr = 1.5 Å and k = 20 kcal/Å^2. This system was then progressively heated to provide the starting configuration at each of the simulated temperatures. During the heating process, the origins of the columnar restraints were continuously updated with each time step based on the average positions of molecules that make up the columns in order to allow the columnar centers of mass to drift while maintaining the columnar structures and to make it possible for the columns to assume a non-hexagonal structure. After reaching a stable temperature, each simulation ran for at least 1.5 ns before all restraints were removed and the systems were allowed to evolve before data collection began. Equilibration times between 5 and 30 ns (appropriate for high temperature isotropic states and low temperature solid states with long relaxation times, respectively) were determined by monitoring density and energy fluctuations in the system and confirming that the volume of the simulated box and the total energy of the system had reached a stable value.

Simulation temperatures were selected in order to obtain a high temperature isotropic phase for each molecule, with the low temperature limit chosen based on the experimental phase transition temperatures of the molecules and the observed behavior of the simulated systems. At each temperature, after equilibration, the simulations were run long enough to capture the key dynamics signatures of the system, with a goal of including between 3 and 5 ns of data in our analysis at each temperature. While fast intracolumn dynamics allow the static structure and certain intracolumn dynamics (e.g., molecular rotations) to be probed over timescales as short as ~100 ps, the slow intercolumn dynamics (i.e., hopping between columns in the mesophase) required substantially longer run times. The target run times were chosen in order to observe a process of substantial interest to us, intercolumn motion with molecules "hopping" between columns in the mesophase (see below for details).

Experimentally, the crystal phases of our compounds tend to have columnar structures, with the crystals having hexagonal or monoclinic symmetry depending on the arrangement of the columns. Therefore, we expected that a significant challenge in this work would be differentiating between a crystal phase and the columnar mesophase. This problem is aggravated by the fact that changes in the alignment of the molecules at a crystal–crystal *or* a crystal–liquid crystal transition will generally cause a change in

Downloaded from http://pubs.aip.org/aip/jcp/article-pdf/doi/10.1063/5.0106722/16552584/134901_1_online.pdf

Published under an exclusive license by AIP Publishing

both static orientational order parameters and the density. The similarity between the crystal and mesophase structures, along with finite size effects, makes it difficult to unambiguously distinguish between them based on the static geometry alone. Therefore, we look for dynamic signatures of liquid-like behavior, specifically focusing on rotational and translational motion within a column, relative motion of columns, and molecular hopping between columns. As will become evident, the observation of dynamic properties provides a powerful tool in the present study. Through the combination of the static columnar structure with these liquid-like dynamic properties, we were able to identify the mesophase.

III. RESULTS

A. Static structure

A direct indicator of a first order phase transition is a change in density. In Fig. 2, the density of each compound is shown at all of the simulated temperatures. With the exception of F5, the systems show two sharp changes in density, the first when they undergo a transition from their low temperature solid states into an intermediate state and another when melting into an isotropic liquid. No such intermediate state is observed in F5, which melts directly into the isotropic phase. Because the full analysis presented below identifies the intermediate state as a columnar liquid crystal mesophase, we will refer to this intermediate state as the *mesophase*.

For F6, F7, and F8, the first drop in density coincides with a small decrease in the orientational order of the molecules. The orientational order was determined by the smallest eigenvalue of the orientational tensor given by[42,43]

$$\mathbf{Q} = \frac{1}{2N}\sum_{i=1}^{N}(3\hat{n}_i \otimes \hat{n}_j - \mathbf{I}), \tag{2}$$

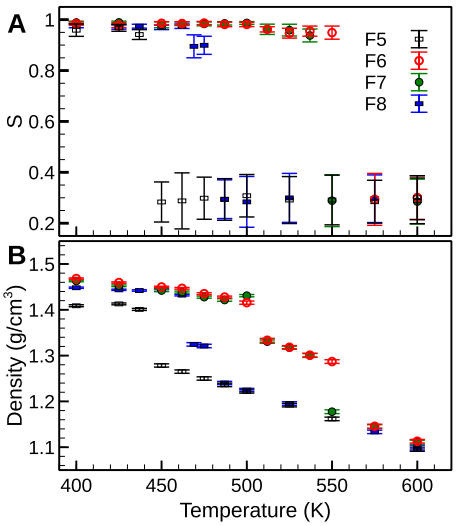

FIG. 2. Evolution of the (a) orientational order parameter, S, and (b) density, as a function of compound and temperature. Except for F5, all the systems have a drop in density that coincides with a small decrease in the order parameter, before the system melts into an isotropic state.

where $\mathbf{I}$ is the identity matrix. The order parameter, S, is defined such that an isotropic material has a value near zero and a perfectly aligned material has a value of one. The columnar structure leads to molecules tending toward a highly cofacial arrangement, with S close to unity in both the low temperature crystalline state and the columnar mesophase. There is a small decrease in S on entering the mesophase. The small change in S is shown in Fig. 2. The reduced order is most pronounced for F8, where S decreases from around 0.95 to 0.85 in the mesophase. For the more planar molecules, F7 and F8, both the crystalline state and the mesophase have S values under 0.1 with only a small decrease in the mesophase. While the S order parameter is affected by the increased disorder of the mesophase, it is far more heavily influenced by the geometries of the molecules and the structure of the crystalline structure. While this quantity is commonly used to describe the columnar mesophase, its utility in identifying a transition between a crystal phase with columnar stacking and the mesophase is limited by the small magnitude of the change in S between the phases.

B. Columns

To study the nature of columnar ordering, we calculate a three dimensional pairwise distribution function, $g(\vec{r})$, which describes the likelihood of a molecule j, whose position is $\vec{r}_j$, located a distance $\vec{r}$ away from a reference molecule i, whose position is $\vec{r}_i$, with $\vec{r}_{ij} = \vec{r}_j - \vec{r}_i$,

$$g(\vec{r}) = \frac{1}{N}\left\langle \frac{1}{\rho}\sum_{i=1}^{N}\sum_{j\neq i}^{N}\delta(\vec{r} - \vec{r}_{ij})\right\rangle, \tag{3}$$

where ρ is the number density of the system and the brackets indicate an ensemble average. The distribution function is subject to the condition that

$$\int_V g(\vec{r})dV = V. \tag{4}$$

In order to study the structure within and between columns, one and two dimensional distributions (parallel and perpendicular to the columnar axis, respectively) were obtained by integrating $g(\vec{r} = x\hat{\mathbf{x}} + y\hat{\mathbf{y}} + z\hat{\mathbf{z}})$ as

$$g(z) = \frac{4}{\pi d^2}\iint g(\vec{r})\theta\left(\frac{d}{2} - \sqrt{x^2 + y^2}\right)dx\,dy, \tag{5}$$

$$g(x,y) = \frac{1}{c}\int g(\vec{r})\theta\left(\frac{c}{2} - |z|\right)dz, \tag{6}$$

where c and d are the average intracolumn and intercolumn spacing, θ is the Heaviside step function, and the lab frame z-axis is taken to be coincident with the columnar axis. In the isotropic state, where there are no columns, we instead prepare analogous distribution functions in the molecular frame to obtain distributions parallel $[g_{\parallel}(z)]$ and perpendicular $[g_{\perp}(x,y)]$ to the individual molecular directors,

$$g_{\parallel}(z) = \frac{L^*}{\delta L}\left\langle \frac{\sum_{j}^{N}\sum_{i\neq j}^{N}\delta(z - |\vec{r}_{ij}\cdot\hat{n}_i|)\theta(d/2 - |\vec{r}_{ij}\times\hat{n}_i|)}{\sum_{j}^{N}\sum_{i\neq j}^{N}\theta(d/2 - |\vec{r}_{ij}\times\hat{n}_i|)}\right\rangle, \tag{7}$$

Downloaded from http://pubs.aip.org/aip/jcp/article-pdf/doi/10.1063/5.0106722/16552584/134901_1_online.pdf

Published under an exclusive license by AIP Publishing

$$g_{\perp}(x,y) = \frac{L^{*2}}{\delta L^2}\left\langle \frac{\sum_{j}^{N}\sum_{i\neq j}^{N}\delta(x-\vec{r_{ij}}\cdot\hat{\mathbf{x}})\delta(y-\vec{r_{ij}}\cdot\hat{\mathbf{y}})\theta(c/2-|\vec{r_{ij}}\cdot\hat{\mathbf{z}}|)}{\sum_{j}^{N}\sum_{i\neq j}^{N}\theta(c/2-|\vec{r_{ij}}\cdot\hat{\mathbf{z}}|)}\right\rangle. \quad (8)$$

The brackets indicate an ensemble average and, due to the lack of columns, c and d are the average intermolecular nearest neighbor separations measured parallel and perpendicular to $\hat{n}$, respectively. The correlation functions in the isotropic phase were limited to a sphere of radius L^* where $\sqrt{L^{*2}+d^2}$ is less than half the minimum dimension of the simulation box and δL^2 is the area of a bin size in the x–y plane (additional histogramming details are given in the supplementary material).

To see correlations between columns, a similar procedure was used as the one to calculate $g(z)$, except with the step function moved such that the integral gives the likelihood of finding a molecule in a neighboring column with a specific z displacement relative to a reference molecule,

$$g'(z,\vec{R}) = \frac{4}{\pi d^2}\iint g(\vec{r})\theta\left(\frac{d}{2}-\left|(\vec{r}-\vec{R})\times\hat{\mathbf{z}}\right|\right)dx\,dy, \quad (9)$$

where $\vec{R}$ is a vector in the x–y plane separating neighboring columns [$g(z) = g'(z,0)$]. The columnar mesophase has hexagonal symmetry, so $g'(z,\vec{R})$ does not depend on which column $\vec{R}$ points to because all neighboring columns are on average identical. While the crystalline states have a columnar structure, they lack hexagonal symmetry, and $g'(z,\vec{R})$ is dependent on the choice of $\vec{R}$.

Representative distribution functions are shown for F8 (liquid crystalline) and F5 (non-liquid crystalline) in Fig. 3. In the mesophase and crystalline states [Figs. 3(b)–3(d)], there is a clear columnar structure that decays slowly, similar to what has been seen elsewhere for dense systems of hard discotic molecules.[14] As the system enters the mesophase, the columns become more disordered (i.e., featuring broader peaks) but still have a clearly defined periodic structure. Intercolumn correlations, $g'(z,\vec{R})$, are shown for two neighboring columns, with $\vec{R}$ vectors marked on the $g(x,y)$ plot [Figs. 3(e) and 3(f)]. At low temperatures (462 K and below for F8, 437 K and below for F5), there are significant correlations between nearby columns, with the structure of the columns depending on $\vec{R}$ [Figs. 3(c) and 3(d)]. Columns within the same row ($\vec{R} = d\hat{\mathbf{y}}$) tend to have coplanar molecules, while those from adjacent rows are offset such that their molecules sit between those of the reference column. This structure, with slight variations, is observed in the crystalline states of all the compounds. In the mesophase, all neighboring columns behave identically, signaling the onset of hexagonal symmetry in the columnar mesophase. In the mesophase, the correlations between columns, $g'(z,\vec{R})$, are greatly reduced and the distribution of molecules from neighboring columns become nearly uniform [Fig. 3(b)]. This de-correlation is a result of columns

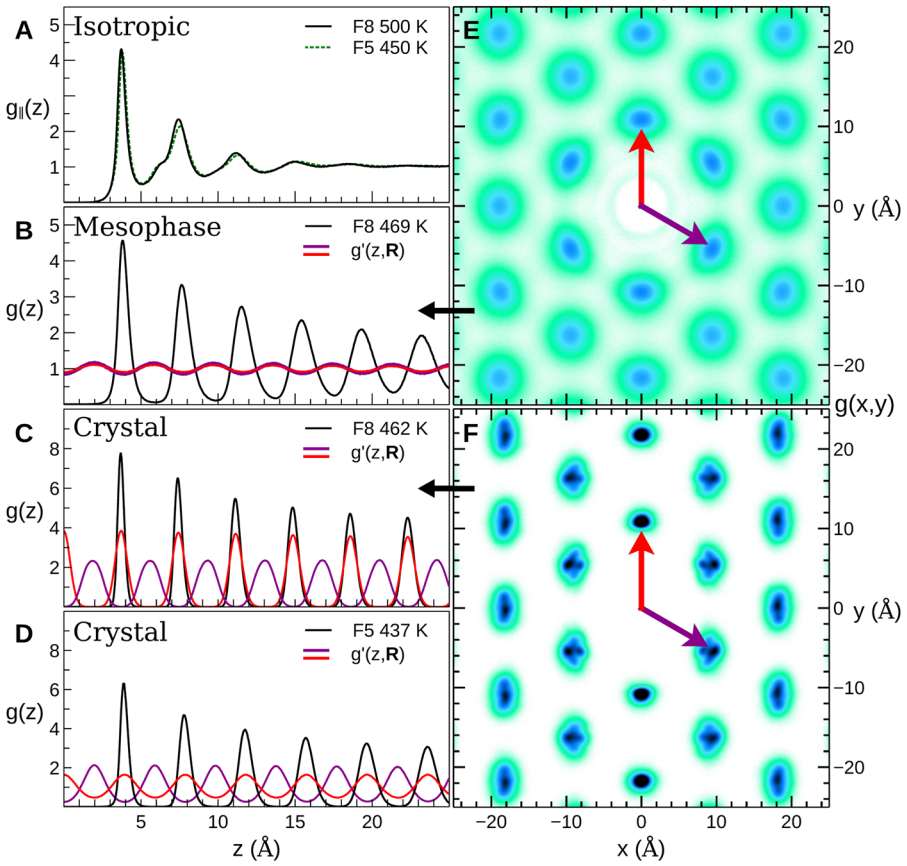

FIG. 3. Pair distribution functions showing structure and arrangement of the columns in the mesophase [(a)–(d) $g(z)$, (e) and (f) $g'(z,\vec{R})$]. The two dimensional plots are for F8, in the crystalline state and the mesophase, and correspond to the $g(z)$ plots as indicated by the short black arrows. The $g(z)$ plots include intercolumn correlations showing the relative positions of molecules from neighboring columns, $g'(z,\vec{R})$, with the vectors $\vec{R}$ marked on the two dimensional plots. In the crystal, the neighboring columns have a low symmetry structure with the position of molecules within columns depending on the relative position of the columns. In the mesophase, these intercolumn correlations are lost and the symmetry of the system increases significantly. This pattern of behavior is seen in all other compounds, except for F5, which lacks the mesophase. Additional results for other compounds and temperatures are collected in the supplementary material.

Downloaded from http://pubs.aip.org/aip/jcp/article-pdf/doi/10.1063/5.0106722/16552584/134901_1_online.pdf

Published under an exclusive license by AIP Publishing

beginning to move relative to one another, with collective molecular motion parallel to the columnar axis. The molecules within a column move together, preserving the intracolumn correlations, $g(z)$, while the relative motion between columns reduces the intercolumn correlations, $g'(z,\vec{R})$. This motion will be discussed in later sections.

C. Cages

In the crystalline state and mesophase, molecular motion is constrained by a cage formed by the neighboring columns and neighboring molecules within the column. Molecules rattle within this steric cage, with displacements that are small relative to the intercolumn and intracolumn spacing. In soft matter systems like ours, these cages dominate the molecular dynamics on the picosecond timescale,[44] which is sufficient for molecules to explore the limits of the cage without escaping from it. In our systems, the typical first passage time for molecules to escape their cages is on the order of nanoseconds, so we are able to view these cages as essentially static structures persisting for hundreds of picoseconds, even in the mesophase. As such, the cages both reflect the static structure of the system (on short timescales) and influence the dynamics of the system across multiple orders of magnitude of time.[14,45] The structure of the cages is a result of the interactions between molecules with their local environment. As a result, the properties of the cages, in the static limit, can provide valuable information about the relationship between the atomic structure of the molecule and the properties of the system.

To see this, we look at the neighboring columns and find the likelihood of there being a nearby column at some point in the molecular frame. We identify neighboring molecules as those that form a Voronoi cell around a molecule (via Voro++[46]). For the purpose of examining intercolumn interactions, we restrict the neighbor list to those adjacent molecules that have a perpendicular displacement from the reference molecule of at least one molecular radius, r_m (to avoid including intracolumn molecules) and those with similar alignment to that of the reference molecule (to avoid including molecules that have left a column and have temporarily become stuck sideways between columns). Specifically, we include those molecules that are part of a Voronoi cell and have

$$|(\vec{r}_i - \vec{r}_j) \times \hat{\boldsymbol{n}}_{\boldsymbol{i}}| \geq r_m, \tag{10}$$

$$\hat{\boldsymbol{n}}_{\boldsymbol{i}} \cdot \hat{\boldsymbol{n}}_{\boldsymbol{j}} \geq 0.5. \tag{11}$$

This restriction limits the molecules included in this analysis to those which make up the surrounding columns. This method of choosing neighbors avoids problems associated with other methods of identifying neighbors, such as taking all molecules within some annulus, which can suffer from the loss of neighbors or inclusion of next nearest neighbors based on brief fluctuations in molecular positions.[47]

For each neighbor identified this way, we find its distance in the x–y plane away from the reference molecule, R_{ij}. To relate the structure of a molecule to the structure of the surrounding cage, we are interested in identifying the portion of the molecule that lies along the line between the molecules.[48] For this, we use an angle λ_{ij}, defined as the angle between $\hat{f}_i$ and $\vec{R}_{ij}$ with the sign of λ_{ij} fixed so that it is positive when $\vec{R}_{ij}$ passes through the reference molecule's monofluorinated ring, as shown in Fig. 4. The angle λ_{ij} is defined in terms of in-plane intermolecular separation, $\vec{R}_{ij}$, and the angle of $\vec{R}_{ij}$ from the x-axis, as

$$\vec{R}_{ij} = \vec{r}_{ij} - (\vec{r}_{ij} \cdot \hat{\mathbf{z}})\hat{\mathbf{z}}, \tag{12}$$

$$\theta_{ij} = \tan^{-1}\left(\frac{\vec{R}_{ij} \cdot \hat{\mathbf{y}}}{\vec{R}_{ij} \cdot \hat{\mathbf{x}}}\right), \tag{13}$$

$$\lambda_{ij} = (\theta_{ij} - \gamma_i)\frac{\hat{n}_i \cdot \hat{\mathbf{z}}}{|\hat{n}_i \cdot \hat{\mathbf{z}}|}, \tag{14}$$

where the dot products in Eq. (14) ensure that the monofluorinated ring is at $\lambda = +120°$.

This angle, λ_{ij}, describes which part of a molecule takes part in an interaction in much the same way that specific close contacts are used to describe molecular crystal structures. The relationship between λ_{ij} and R_{ij} also carries information about any preferred orientation of a molecule relative to its neighbors and the ease with which a molecule might spin and rattle within its cage. To explore this, we calculate a potential of mean force (PMF) for the intermolecular cage based on the probability of a neighboring molecule being a distance R away from a reference molecule at a particular angle λ,

$$P(R,\lambda) = \frac{1}{N_0}\langle\delta(R - R_{ij})\delta(\lambda - \lambda_{ij})\rangle, \tag{15}$$

with the prefactor defined such that

$$\iint P(R,\lambda)RdRd\lambda = 1 \tag{16}$$

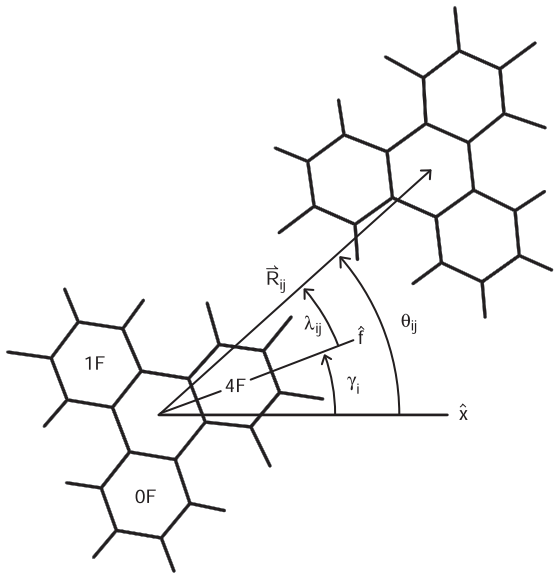

FIG. 4. Illustration of the quantities used to relate the structure of a molecule to its neighbors. The angle λ_{ij} identifies the area of a molecule that lies on the line between it and a neighboring molecule, R_{ij}. The perfluorinated ring corresponds to $\lambda_{ij} = 0$, and the mono- and nonfluorinated rings are at $\lambda_{ij} = \pm 120°$, respectively.

Downloaded from http://pubs.aip.org/aip/jcp/article-pdf/doi/10.1063/5.0106722/16552584/134901_1_online.pdf

Published under an exclusive license by AIP Publishing

and the brackets indicating an ensemble average of all neighbors, as defined above, for each molecule. The PMF, $U(\lambda, R)$, is then determined from the Boltzmann factor,[14,49]

$$P(\lambda, R) \propto \exp\left(-\frac{U(\lambda, R)}{k_B T}\right). \tag{17}$$

The PMF for the simulated molecules is shown in Fig. 5 in the crystalline state and, where applicable, in the mesophase. In the crystal, $U(\lambda, R)$ has six potential wells with $\sim 3k_B T$ barriers between them [Figs. 5(b), 5(d), 5(f), and 5(h)], and these barriers are reduced to nearly one $k_B T$ in the mesophase [Figs. 5(c), 5(e), and 5(g)]. This transition also increases the symmetry of $U(\lambda, R)$ from the approximate threefold symmetry of the crystal to a near perfect sixfold symmetry in the mesophase, with slight deviations. Specifically, for all simulated mesogens, the minimum of $U(\lambda, R)$ occurs near the bay opposite of the perfluorinated ring ($\lambda = 180^\circ$) and the barriers are greatest near the bay between the perfluorinated and monofluorinated rings ($\lambda = 60^\circ \pm 30^\circ$). The barriers are especially small (under $k_B T$) for F8, possibly because the fluorine is sheltered within the bay, unlike F6 and F7, which have their fifth fluorine at an extreme position of the periphery where it may encounter steric interactions with neighboring molecules. Additionally, when the fluorine is in the 8 or 7 (and to a lesser extent 6) position, it reduces the dipole moment of tetrafluorotriphenylene. This may make the sixfold symmetry of the mesophase more obtainable as alignment between molecules is less likely to be dominated by twofold symmetric charge–charge interactions.

We are also able to compute an expectation value of the intercolumn separation as a function of λ,

$$\langle R(\lambda) \rangle = \frac{\int P(R, \lambda) R^2 dR}{\int P(R, \lambda) R dR}. \tag{18}$$

This describes an effective "shape" of the molecules based on their interaction with their cages. At low temperatures, $\langle R(\lambda) \rangle$ has a gear-like structure with three "teeth" that extend roughly an Ångstrom beyond the average intercolumn distance [Fig. 5(a)]. This gear-like shape hinders molecular rotation as it requires coordinated motion from multiple columns, which introduces the possibility of frustration where three columns meet, or results in gears "grinding" against their neighbors.[50] In the mesophase, $\langle R(\lambda) \rangle$ is not quite symmetric in λ, but it lacks the abrupt steps found in the crystalline state. Instead, $\langle R(\lambda) \rangle$ is slightly greater near the rings and, like triphenylene, resembles a rounded triangle. Without the teeth, molecules are better able to rotate independently of their neighbors.

It is important to recall that the PMF and related quantities are static quantities. The position and depth of the minima in the PMF can result from motion of the molecules that cause their orientations to evolve over time or from a distribution of molecular orientations that are frozen in place. To differentiate between a glass and a liquid crystal requires us to examine the dynamic properties of the system.

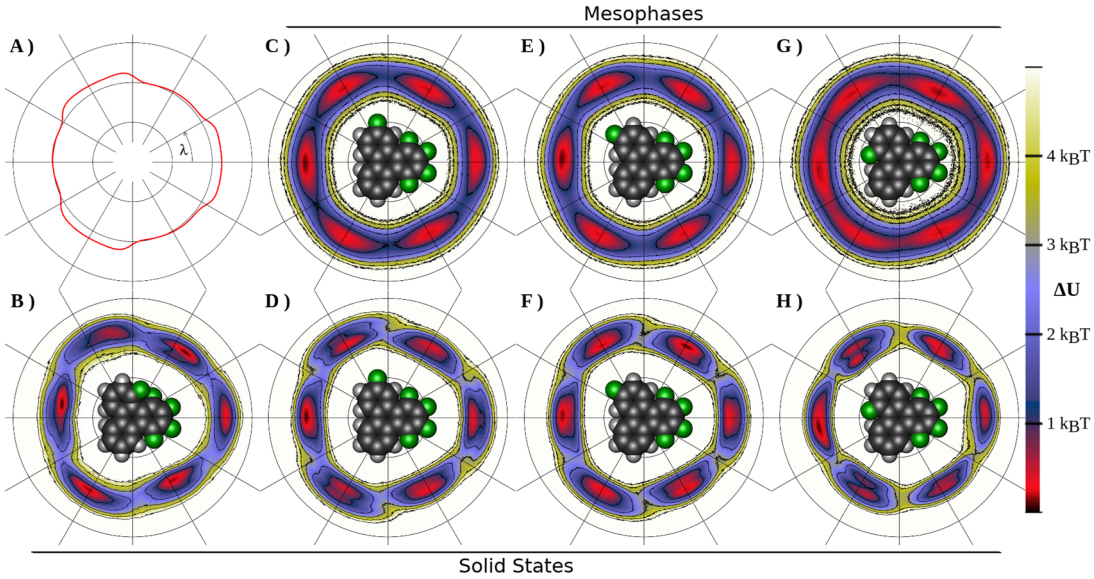

FIG. 5. Potential of mean force of the nearby columns in the crystalline state and mesophase of all four compounds [(b) F5 at 425 K, (c) and (d) F6 at 500 and 525 K, (e) and (f) F7 at 500 and 512 K, (g) and (h) F8 at 462 and 469 K]. (a) Expected intercolumn distance as a function of λ for F6 at 500 K. (b)–(h) PMF in the crystal and mesophase. For all molecules, the crystal [(b), (d), (f), and (h)] features six potential wells with $\sim 3k_B T$ barriers between them. These barriers are reduced to $\lesssim k_B T$ in the mesophase [(c), (e), and (g)]. In the mesophase, the local minima are all at approximately the same nearest neighbor distance, while the crystal has minima with separation distances that are dependent on the molecular geometry. The intercolumn distance shown in (a) is typical of the crystalline states of all molecules and features a gear-like shape with intercolumn distances changing by ~1 Å. This gear-like shape requires coordinated motion between columns in order for molecules to rotate as columns need to move out of the way of the "teeth."

Downloaded from http://pubs.aip.org/aip/jcp/article-pdf/doi/10.1063/5.0106722/16552584/134901_1_online.pdf

Published under an exclusive license by AIP Publishing

D. Dynamic structure

The liquid-like properties of the mesophase require the presence of several key dynamic properties, each of which is associated with the molecules gaining a degree of freedom. Specifically, molecules gain rotational freedom about the z-axis while within their columns, the columns move relative to one another with motion parallel to the columnar axes, and molecules occasionally hop between adjacent columns. To identify the first two, we look for the onset of specific types of diffusive motion. For the third, we look for molecular displacements corresponding to intercolumn hopping.

1. Diffusion

In the columnar mesophase, the disk-shaped molecules are able to spin about their molecular director. We track these rotations via the angle γ made between $\hat{f}$ (projected into the x–y plane) and $\hat{\mathbf{x}}$ (illustrated in Fig. 4). The distribution of angular displacements is given by the autocorrelation function,

$$\Gamma_s(\gamma, t) = \frac{1}{N}\left\langle \sum_{i=1}^{N} \delta(\gamma - |\gamma_i(t+t_0) - \gamma_i(t_0)|) \right\rangle, \tag{19}$$

which is the probability that a molecule has spun an angle γ about the columnar axis after a time, t. Similarly, the mean squared angular displacement is

$$\langle \gamma(t)^2 \rangle = \frac{1}{N}\left\langle \sum_{i=1}^{N} (\gamma_i(t+t_0) - \gamma_i(t_0))^2 \right\rangle. \tag{20}$$

In both cases, the brackets indicate an ensemble average. In order to find these displacements, the angles are "unrolled" such that $\gamma_i(t)$ is continuous and may have values exceeding 2π.

In both the isotropic state and the mesophase, the rotations become diffusive, with the mean squared angular displacement increasing linearly in time on timescales greater than 10 ps [Fig. 6(a)]. Over large timescales, there is angular diffusion in the crystalline state, with molecules making infrequent but large rotations. The distribution of angular displacements, $\Gamma_s(\gamma, t)$ [Fig. 6(b)], shows discrete rotations of 120° in the crystal. In the mesophase, there is a large increase in the rotational freedom, with the rotational motion resembling the isotropic state but with a bias toward discrete 60° rotations. This marks a transition from rotations governed by the (approximate) threefold symmetry of the molecules to the sixfold symmetry of the columnar array, similar to the transition noted above in the PMFs. We have found that the discrete 60° rotations are one of the most robust indicators of the mesophase as this type of motion is unique to the liquid crystal and is not associated with any slow relaxation dynamics found in the crystalline states as they approach equilibrium.

Similar rotational dynamics have been observed experimentally in conventional tailed DLCs, with discrete rotations occurring in glass-like solid states, with the jumps reflecting the symmetry of the molecules, and slow rotations present in the mesophase.[51–53] Without the presence of long tails, the process of rotating about the columnar axis is presumably greatly simplified and the tail-free DLCs are able to spin with relative ease.

Since part of our aim is to clearly differentiate a columnar mesophase from other possible phases, we note that the onset of rotational freedom is observed in the isotropic state as well as in plastic crystals.[54,55] The isotropic state lacks the structure observed in the mesophase, among other things, and is easily identified. Plastic crystals, however, have similar rotational motion but lack translational freedom. To identify the onset of translational freedom, we look at the mean squared displacements of motion parallel and perpendicular to the columns as a function of time, averaged over all molecules,

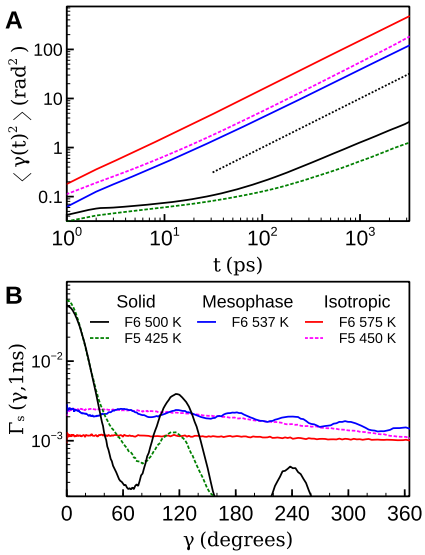

FIG. 6. (a) Mean square angular displacement, $\langle \gamma(t)^2 \rangle$, and (b) distribution of angular displacements, $\Gamma_s(\gamma, t)$, for F6 at 500 (crystal), 537 (mesophase), and 575 K (isotropic) as well as the non-liquid crystal F5 in the crystal and isotropic states. The black dotted line in the top plot is a reference for diffusive rotational motion, wherein the mean squared angular displacement grows linearly in time. Rotational excursions in the crystalline state are restricted to small amplitude rotations and infrequent 120° rotations. On entering the mesophase, the molecules rotate much more freely, closely resembling the rotational freedom of the isotropic state, except that the rotations tend to occur in discrete 60° steps. Similar behavior is observed in F7 and F8. Additional results for other compounds and temperatures are collected in the supplementary material.

$$\langle r_{\parallel}(t)^2 \rangle = \frac{1}{N}\left\langle \sum_{i=1}^{N} |(\vec{r}_i(t+t_0) - \vec{r}_i(t_0)) \cdot \hat{\mathbf{z}}|^2 \right\rangle, \tag{21}$$

$$\langle r_{\perp}(t)^2 \rangle = \frac{1}{N}\left\langle \sum_{i=1}^{N} |(\vec{r}_i(t+t_0) - \vec{r}_i(t_0)) \times \hat{\mathbf{z}}|^2 \right\rangle. \tag{22}$$

Under normal, i.e., Fickian, diffusion, a particle diffusing in n dimensions has a mean squared displacement that grows like nDt, where D is the diffusion coefficient. This is the case for our compounds at high temperatures in the isotropic state (Fig. 7, F7 at 550 K and F5 at 450 K). In this limit, there is uniform motion in all directions and the translational motion in the system can be described with a single diffusion coefficient.

In the low temperature crystal state, the molecular motion is severely restricted. Molecules are frozen in place and vibrate around an equilibrium position. These vibrations result in a coherent oscillation evident in the mean squared displacement. This can be seen

Downloaded from http://pubs.aip.org/aip/jcp/article-pdf/doi/10.1063/5.0106722/16552584/134901_1_online.pdf

Published under an exclusive license by AIP Publishing

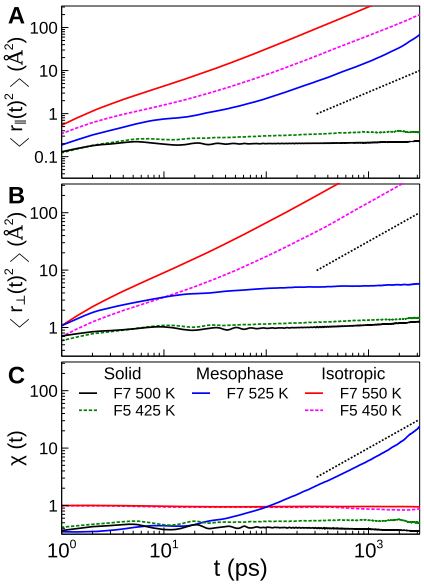

FIG. 7. The mean squared displacements of molecules (a) parallel and (b) perpendicular to the columns, and (c) twice their ratio, $\chi(t)$. In the solid state (425 K for F5 and 500 K for F7), motion is confined both parallel and perpendicular to the columns. In the mesophase (F7 at 525 K), perpendicular motion is still confined though the molecules began to move parallel to the columnar axis. The combination of restricted perpendicular motion and diffusion along the columnar axis results in $\chi(t) \sim t$. This behavior is absent in F5, which melts directly into the isotropic state (450 K for F5 and 550 K for F7) where the isotropic diffusion makes χ tend to unity. In all plots, the dotted line is a reference indicating diffusive motion. The limited super-diffusive behavior of $\langle r_{\parallel}(t)^2 \rangle$ of F7 at 525 K is not a statistically significant feature of the mean squared displacement. Results for other compounds and temperatures are collected in the supplementary material.

in Fig. 7 for F7 at 500 K and F5 at 425 K. Any growth in the mean squared displacement at these temperatures is small, compared to the intermolecular spacing, and sublinear in time. This confined sub-diffusive motion occurs both parallel and perpendicular to the columns [Figs. 7(a) and 7(b)], with slightly different properties reflecting the anisotropy of the columnar geometry. Specifically, $\langle r_{\perp}(t)^2 \rangle$ is generally larger than $\langle r_{\parallel}(t)^2 \rangle$ due to the difference in intercolumn and intracolumn spacings, limiting the maximum extent of motion in the low temperature solid state.

The liquid crystal mesophase has properties comparable to each of these limits. The motion parallel to the columns becomes diffusive on timescales greater than 100 ps, and it closely resembles the motion found in the isotropic state [F7 at 525 K in Fig. 7(a)]. This diffusive motion is a collective process of the columns, with columns moving relative to one another while maintaining their internal structure. At the same time, perpendicular motion is limited by neighboring columns and $\langle r_{\perp}(t)^2 \rangle$ [F7 at 525 K in Fig. 7(b)] approaches a value based on the extent to which the cage formed by the neighboring columns allows it. This resembles the restricted motion seen at low temperatures, except that it lacks a coherent structure. Molecules do not vibrate around a fixed point, but they rattle around their cages, fully exploring the space available to them. This leads to an increase in $\langle r_{\perp}(t)^2 \rangle$ (relative to the solid phase) and the development of a smooth plateau.

These scenarios (confined vibrations in the crystal, one dimensional diffusion of the columns in the mesophase, and three dimensional diffusion as an isotropic liquid) can readily be distinguished based on the ratio of the mean squared displacements,

$$\chi(t) = \frac{2\langle r_{\parallel}(t)^2 \rangle}{\langle r_{\perp}(t)^2 \rangle}. \tag{23}$$

The factor of two accounts for the difference in dimensionality of motion parallel and perpendicular to the columns. In the isotropic phase, $\chi(t)$ tends to unity for isotropic diffusion. In the columnar mesophase, over timescales where molecules are confined to their columns, the one dimensional diffusion along the columnar axis results in $\chi(t) \sim t$ [F7 at 525 K in Fig. 7(c)]. The dynamic anisotropy, which results in this linear growth of $\chi(t)$, also created the de-correlation between columns, $g'(z, \vec{R})$, which we saw earlier [Fig. 3(b)]. The crystalline phases have a static anisotropy based on a difference in diffusion coefficients governing motion perpendicular and parallel to the columns but with the same mechanism of motion, giving an essentially constant value of χ.

Over sufficiently long timescales in the mesophase, molecules are able to escape their cages. At timescales less than this cage escape time, molecular motion perpendicular to the column is restricted, as is the case of F7 at 525 K [Fig. 7(b)]. At this temperature, very few molecules are able to escape their cages and $\langle r_{\perp}(t)^2 \rangle$ is essentially flat at long times. At higher temperatures (but still in the mesophase), there is an increase in the ability of molecules to escape their cages and there is a corresponding increase in intercolumn motion on long timescales.

This crossover time marks the typical time required for a molecule to escape its cage[14,45] and the shift in the mechanism driving the perpendicular motion from rattling within the cages to hopping between them. This can be seen for F6 in Fig. 8, where $\langle r_{\perp}^2 \rangle$ has a temperature dependent increase at times greater than 1 ns (similar results are seen in F7 and F8 in the mesophase). The crossover time varies with compound and temperature, and it occurs near the long time limit of our simulations, which limits the detail we are able to provide about this transition. The hopping causes an uptick in $\langle r_{\perp}^2 \rangle$, as the time dependence of these two modes of

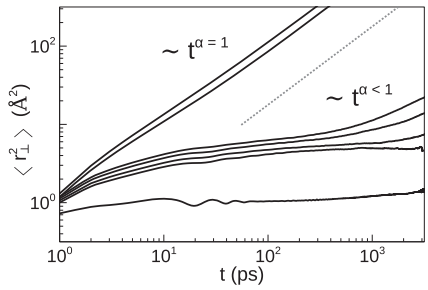

FIG. 8. Mean squared displacement perpendicular to the columns for F6 between 500 (lowest curve) and 600 K (highest curve, in ascending order of temperature). At sufficiently high temperatures, motion is restricted in the mesophase at timescales less than a nanosecond as molecules are confined in their columns. At longer timescales, intercolumn hopping leads to an increase in sub-diffusive motion perpendicular to the columns. The short dotted line is a reference for diffusive motion.

Downloaded from http://pubs.aip.org/aip/jcp/article-pdf/doi/10.1063/5.0106722/16552584/134901_1_online.pdf

Published under an exclusive license by AIP Publishing

molecular motion differs. The limited motion of molecules rattling in cages is augmented by the anomalous (sublinear) diffusion driven by molecules hopping between columns.[56] This results in the system having a time dependent diffusion coefficient, which, in turn, results from the vastly different timescales of these types of motion, and the dependence of the intermittent hopping events on cooperation between columns neighboring columns.[45,57]

2. Hopping

To better understand the hopping between columns, we use the self-van Hove function,[58,59] $G_s(\vec{r},t)$, a time dependent autocorrelation function describing the probability that a particle has moved some amount $\vec{r}$ after a time, t. Again, we break this into separate components for motion parallel (z) or perpendicular (ρ) to the columnar axis,

$$G_{s,\parallel}(z,t) = \frac{1}{N}\left\langle \sum_{i=1}^{N} \delta(z - |(\vec{r}_i(t+t_0) - \vec{r}_i(t_0)) \cdot \hat{\mathbf{z}}|) \right\rangle, \tag{24}$$

$$G_{s,\perp}(\rho,t) = \frac{1}{2\pi N}\left\langle \sum_{i=1}^{N} \delta(\rho - |(\vec{r}_i(t+t_0) - \vec{r}_i(t_0)) \times \hat{\mathbf{z}}|) \right\rangle. \tag{25}$$

For freely diffusing liquids, similar to our systems in the isotropic state, these functions can be expected to take the form of Gaussians with widths proportionate to $\sqrt{Dt}$, where D is the diffusion coefficient. At low temperatures, the maximum extent of molecular motion on short timescales is restricted by the surrounding cage, and both $G_{s,\parallel}$ and $G_{s,\perp}$ are restricted to small values reflecting the size of the cage and may exhibit non-Gaussian behavior as a result of the anisotropy of the system,[60] with the dynamics of columnar liquid crystals being influenced by the intermolecular cage and intercolumn motion.[14,61]

As shown in Fig. 9, we see both of these behaviors at the temperature extremes of all of our compounds. In the columnar mesophase, and only in the mesophase, there is an additional feature in the $G_{s,\perp}(\rho,t)$ distributions, which develop a bump near $\rho \sim 11$ Å for timescales greater than 1 ns [F8 at 475 K in Fig. 9(a)]. This distance corresponds to the intercolumn separation; therefore, this feature is the result of molecules escaping their cages and joining a neighboring column. We observe that both the diffusion along the columnar axis and intercolumn hopping begin at the same temperature, with intercolumn hopping rates increasing at higher temperatures (just as the perpendicular motion at long times increased with temperature for F6 in Fig. 8). These phenomena can be expected to be synergistic, for example, density fluctuations that create vacancies amenable to intercolumn hops likely benefit from the relative motion of neighboring columns.

We can visualize the hops between columns in more detail by examining the average displacement of each molecule,

$$\langle \vec{r}_i(t) \rangle = \langle \vec{r}_i(t+t_0) - \vec{r}_i(t_0) \rangle, \tag{26}$$

averaged over its trajectory. The in-plane component of these is shown in Fig. 9(c), where the molecular displacements clearly show molecules rattling in place on short timescales and jumping between neighboring columns over long timescales. The exact nature of these intercolumn hops and how they are influenced by the molecular structure are of considerable interest. The hops themselves are short, in terms of both distance traveled and duration. Typical hop durations are on the order of tens of picoseconds, with molecules moving directly between neighboring columns. One such hopping event is shown in Fig. 10. The hopping process requires cooperative motion between two (or more) columns in order to form a vacancy in the adopting column. Midway through the process, molecules from both the originating column and adopting column have significant cofacial overlap with the hopping molecule, which briefly forms a sort of bridge between the columns. Molecular transitions between columns are certainly not restricted to tail-free DLCs, but the lack of tails is expected to greatly affect the hopping process. Without tails, the molecules are much smaller, and accordingly, they are able to complete the transition in a much shorter time and are able to maintain core–core contact throughout the entire hopping event.

In addition to these quick short ranged hops, we observe some longer-lived "orphan" molecules that spend relatively long

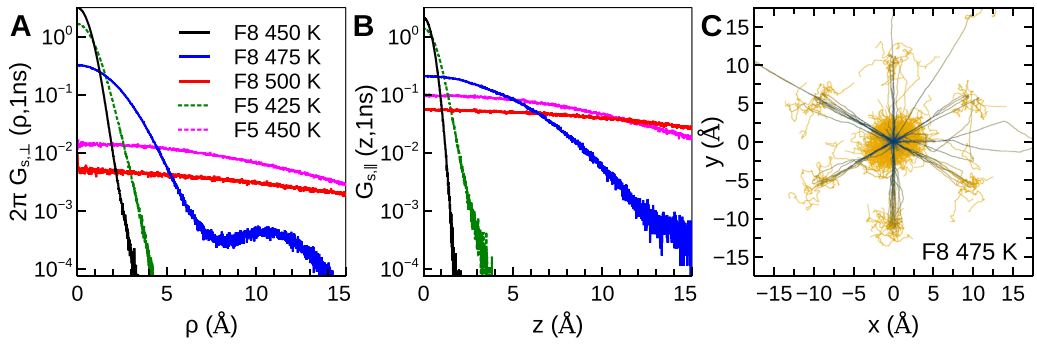

FIG. 9. Self-van Hove functions with a 1 ns time separation, (a) $G_{s,\parallel}(z,t)$ and (b) $2\pi G_{s,\perp}(\rho,t)$, for F5 at 425 K (crystal) and 450 K (isotropic) and F8 at 450 (crystal), 475 (mesophase), and 500 K (isotropic). (c) The average displacement in the x–y plane for each molecule of F8 at 475 K (darker colors correspond to shorter time scales). On entering the mesophase, the molecular motion parallel to the columns increases as columns begin to slide past each other. At the same time, the motion perpendicular to the columns is augmented by occasional "hops" between columns, resulting in the second peak in $G_{s,\perp}$ at a value of $\rho \approx 11$ Å, corresponding to the intercolumn distance. These hops are shown in the plot of the molecular displacements where we see the molecules making direct hops between neighboring columns. The hops are rare events of brief duration, with around ten intercolumn hops per nanosecond in our systems and the hops themselves lasting tens of picoseconds.

Downloaded from http://pubs.aip.org/aip/jcp/article-pdf/doi/10.1063/5.0106722/16552584/134901_1_online.pdf

Published under an exclusive license by AIP Publishing

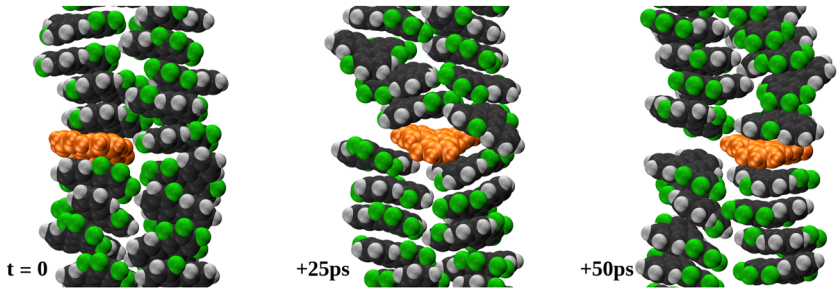

FIG. 10. An F8 molecule hopping between two adjacent columns at 475 K. Before and after the transition has occurred, both the columns are reasonably well ordered, with a high degree of cofacial alignment. During the transition, the mobile molecule maintains its alignment with the columnar axes while the molecules immediately surrounding it deviate from this alignment for the duration of the hop.

times intercalated between columns. These molecules adopt a sideways orientation with their molecular director perpendicular to the columnar axes. In this orientation, they are able to move along a column or slip between columns, before being adopted by another column. On average, these molecules spend ~100 ps between the columns, with some remaining there for over a nanosecond. These orphan molecules have an increased mobility parallel to the columns and are in part responsible for the long tail in $G_{s,\parallel}$ in Fig. 9.

Both these types of intercolumn transition are rare events, requiring long timescales in order to study. Intercolumn hopping has been seen in coarse-grained simulations where the necessary timescales are accessible, but the information that can be gathered about the conditions surrounding the hops is limited.[14,17,19,61] The exact circumstances that lead to a molecule leaving or entering a column are the subject of future work to study how the hopping process depends on the relative position and orientation of the hopping molecule and its neighbors. Ultimately, a detailed knowledge of these hopping events may be useful for informing the design of additional tail-free mesogens.

IV. CONCLUSIONS

We carried out a series of all-atom simulations of a set of four tail-free discotic molecules, two of which are known experimentally to be mesogens. Using rigid molecules and nonpolarizable force fields, we observe signatures of the columnar mesophase in some *but not all* of our compounds. We identify three degrees of freedom present in the columnar mesophase: (nearly) free rotation of molecules defined by discrete 60° rotations within their columns, one dimensional translational freedom with molecular motion parallel to the columnar axis, and the ability for molecules to make discrete hops between columns. Tail-free discotic liquid crystals are known, experimentally, to have complicated phase sequences, often forming glasses and plastic crystals or possessing multiple crystal–crystal transitions.[7,8] This complicated behavior may be related to these degrees of freedom becoming accessible in the system, resulting in the formation of plastic crystals (with rotational but not translational freedom) and liquid crystalline mesophases (with rotational and translational freedom). A more complete understanding of the properties that allow the tail-free DLCs to manifest a mesophase will give us not just a better understanding of this niche group of molecules but also a clearer understanding of the prerequisites of the columnar mesophase more generally.

To understand the relevant timescales that govern these various types of motion, it is important to put them in context with other properties of the materials. DLCs are known to support quasi-one dimensional charge transport based on charges hopping between molecules along the columns, with typical charge mobilities[2,62] between 10^{-5} and 10^{-2} $cm^2\ V^{-1}\ s^{-1}$. This corresponds to a charge dwell time (i.e., the time charges spend localized on a molecule between hops) of up to hundreds of picoseconds. Over these timescales, there is only limited translational motion, but there is a possibility for significant molecular rotation. Additionally, while intercolumn motion becomes diffusive only at times exceeding a nanosecond, the process of molecules jumping between columns (and their neighbors reorganizing themselves post-jump) occurs on timescales comparable to the charge hopping dwell times. This describes a picture where there is substantial molecular motion occurring during the charge conduction process. This is in contrast to conventional DLCs, which, owing to their slower dynamics, appear to have static cores on these timescales.[63]

The tail-free compounds, both mesogenic and otherwise, are great candidates for further study due to their simple structure and the large effect that a small structural change can induce. In particular, F6 and F8 are an ideal test case for more advanced models to produce mesogenic behavior in F8 *but not* F6. Our present model fails the second part of this test. With this in mind, we encourage future work with these physically interesting and easily modeled molecules.

SUPPLEMENTARY MATERIAL

See the supplementary material for molecular structures and partial charges used in this work and for additional data on pair correlation functions $[g(z), g'(z,\vec{R})]$, mean squared displacements $(\langle \gamma^2(t)\rangle, \langle r_\parallel^2(t)\rangle, \langle r_\perp^2(t)\rangle)$, and van Hove functions $[\Gamma_s(\gamma,t), G_{s,\parallel}(z,t), G_{s,\perp}(\rho,t)]$ for all compounds.

ACKNOWLEDGMENTS

We gratefully acknowledge the support of the National Science Foundation, Grant No. 1809536. This work used the Extreme

Downloaded from http://pubs.aip.org/aip/jcp/article-pdf/doi/10.1063/5.0106722/16552584/134901_1_online.pdf

Published under an exclusive license by AIP Publishing

Science and Engineering Discovery Environment (XSEDE), which is supported by National Science Foundation Grant No. ACI-1548562. Resources used include both bridges and Bridges-2, at the Pittsburgh Supercomputing Center, Project No. DMR200072.

AUTHOR DECLARATIONS

Conflict of Interest

The authors have no conflicts to disclose.

Author Contributions

M. Powers: Conceptualization (equal); Data curation (equal); Formal analysis (equal); Investigation (equal); Methodology (equal); Visualization (equal); Writing – original draft (equal); Writing – review & editing (equal). **R. J. Twieg**: Conceptualization (equal); Funding acquisition (equal); Project administration (equal); Writing – review & editing (equal). **J. Portman**: Conceptualization (equal); Funding acquisition (equal); Methodology (equal); Project administration (equal); Supervision (equal); Validation (equal); Writing – review & editing (equal). **B. Ellman**: Conceptualization (equal); Funding acquisition (equal); Methodology (equal); Project administration (equal); Supervision (equal); Validation (equal); Writing – review & editing (equal).

DATA AVAILABILITY

The data that support the findings of this study are available from the corresponding author upon reasonable request.

REFERENCES

[1]S. Chandrasekhar, "Columnar, discotic nematic and lamellar liquid crystals: Their structures and physical properties," in *Handbook of Liquid Crystals Set* (Wiley, 1998), Chap. VIII, p. 749.
[2]T. Wöhrle, I. Wurzbach, J. Kirres, A. Kostidou, N. Kapernaum, J. Litterscheidt, J. C. Haenle, P. Staffeld, A. Baro, F. Giesselmann, and S. Laschat, "Discotic liquid crystals," Chem. Rev. **116**, 1139 (2016).
[3]S. Laschat, A. Baro, N. Steinke, F. Giesselmann, C. Hägele, G. Scalia, R. Judele, E. Kapatsina, S. Sauer, A. Schreivogel, and M. Tosoni, "Discotic liquid crystals: From tailor-made synthesis to plastic electronics," Angew. Chem., Int. Ed. **46**, 4832 (2007).
[4]S. Sergeyev, W. Pisula, and Y. H. Geerts, "Discotic liquid crystals: A new generation of organic semiconductors," Chem. Soc. Rev. **36**, 1902 (2007).
[5]R. Termine and A. Golemme, "Charge mobility in discotic liquid crystals," Int. J. Mol. Sci. **22**, 877 (2021).
[6]M. Sorai and K. Saito, "Alkyl chains acting as entropy reservoir in liquid crystalline materials," Chem. Rec. **3**, 29 (2003).
[7]S. Basurto, S. García, A. G. Neo, T. Torroba, C. F. Marcos, D. Miguel, J. Barberá, M. B. Ros, and M. R. de la Fuente, "Indene and pseudoazulene discotic liquid crystals: A synthetic and structural study," Chem. - Eur. J. **11**, 5362 (2005).
[8]R. J. Twieg, B. Ellman, Z. Li, M. Powers *et al.*, "Fluorinated tail-free triphenylene discotic liquid crystals" (unpublished) (2022).
[9]F. M. Van Der Kooij, K. Kassapidou, and H. N. W. Lekkerkerker, "Liquid crystal phase transitions in suspensions of polydisperse plate-like particles," Nature **406**, 868 (2000).
[10]J. A. C. Veerman and D. Frenkel, "Phase behavior of disklike hard-core mesogens," Phys. Rev. A **45**, 5632 (1992).
[11]H. Azzouz, J. M. Caillol, D. Levesque, and J. J. Weis, "Phase behavior of parallel cut spheres. Monte Carlo and integral equation results," J. Chem. Phys. **96**, 4551 (1992).
[12]M. Marechal, A. Cuetos, B. Martínez-Haya, and M. Dijkstra, "Phase behavior of hard colloidal platelets using free energy calculations," J. Chem. Phys. **134**, 094501 (2011).
[13]A. Cuetos, M. Dennison, A. Masters, and A. Patti, "Phase behaviour of hard board-like particles," Soft Matter **13**, 4720 (2017).
[14]A. Patti, S. Belli, R. van Roij, and M. Dijkstra, "Relaxation dynamics in the columnar liquid crystal phase of hard platelets," Soft Matter **7**, 3533 (2011).
[15]A. P. J. Emerson, G. R. Luckhurst, and S. G. Whatling, "Computer simulation studies of anisotropic systems," Mol. Phys. **82**, 113 (1994).
[16]M. A. Bates and G. R. Luckhurst, "Computer simulation studies of anisotropic systems. XXVI. Monte Carlo investigations of a Gay–Berne discotic at constant pressure," J. Chem. Phys. **104**, 6696 (1996).
[17]O. Cienega-Cacerez, J. A. Moreno-Razo, E. Díaz-Herrera, and E. J. Sambriski, "Phase equilibria fluid structure and diffusivity of a discotic liquid crystal," Soft Matter **10**, 3171–3182 (2014).
[18]R. Berardi, S. Orlandi, and C. Zannoni, "Columnar and interdigitated structures from apolar discotic mesogens with radial dipoles: A Monte Carlo study," Liq. Cryst. **32**, 1427–1436 (2005).
[19]R. Busselez, C. V. Cerclier, M. Ndao, A. Ghoufi, R. Lefort, and D. Morineau, "Discotic columnar liquid crystal studied in the bulk and nanoconfined states by molecular dynamics simulation," J. Chem. Phys. **141**, 134902 (2014).
[20]G. Cinacchi, R. Colle, and A. Tani, "Atomistic molecular dynamics simulation of hexakis(pentyloxy)triphenylene: Structure and translational dynamics of its columnar state," J. Phys. Chem. B **108**, 7969 (2004).
[21]D. Andrienko, V. Marcon, and K. Kremer, "Atomistic simulation of structure and dynamics of columnar phases of hexabenzocoronene derivatives," J. Chem. Phys. **125**, 124902 (2006).
[22]P. L. Cristinziano and F. Lelj, "Atomistic simulation of discotic liquid crystals: Transition from isotropic to columnar phase example," J. Chem. Phys. **127**, 134506 (2007).
[23]L. Muccioli, R. Berardi, S. Orlandi, M. Ricci, and C. Zannoni, "Molecular properties and stacking of 1-substituted hexaalkoxy triphenylenes," Theor. Chem. Acc. **117**, 1085 (2007).
[24]S. Orlandi, L. Muccioli, M. Ricci, R. Berardi, and C. Zannoni, "Core charge distribution and self assembly of columnar phases: The case of triphenylenes and azatriphenylenes," Chem. Cent. J. **1**, 15 (2007).
[25]V. Marcon, T. Vehoff, J. Kirkpatrick, C. Jeong, D. Y. Yoon, K. Kremer, and D. Andrienko, "Columnar mesophases of hexabenzocoronene derivatives. I. Phase transitions," J. Chem. Phys. **129**, 094505 (2008).
[26]Y. Olivier, L. Muccioli, V. Lemaur, Y. H. Geerts, C. Zannoni, and J. Cornil, "Theoretical characterization of the structural and hole transport dynamics in liquid-crystalline phthalocyanine stacks," J. Phys. Chem. B **113**, 14102–14111 (2009).
[27]L. A. Haverkate, M. Zbiri, M. R. Johnson, B. Deme, F. M. Mulder, and G. J. Kearley, "Conformation, defects, and dynamics of a discotic liquid crystal and their influence on charge transport," J. Phys. Chem. B **115**, 13809 (2011).
[28]F. Camerel, F. Barrière, and O. Jeannin, "Simulation of SAXS patterns of hexa-*n*-alkoxy-2,3,6,7,10,11-triphenylene mesophase," Liq. Cryst. **45**, 698 (2018).
[29]M. Valiev, E. J. Bylaska, N. Govind, K. Kowalski, T. P. Straatsma, H. J. J. van Dam, D. Wang, J. Nieplocha, E. Aprà, T. L. Windus, and W. A. de Jong, "NWChem: A comprehensive and scalable open-source solution for large scale molecular simulations," Comput. Phys. Commun. **181**, 1477 (2010).
[30]M. J. Frisch, G. W. Trucks, H. B. Schlegel, G. E. Scuseria *et al.*, Gaussian 16 Revision C.01, Gaussian, Inc., Wallingford, CT, 2016.
[31]U. C. Singh and P. A. Kollman, "An approach to computing electrostatic charges for molecules," J. Comput. Chem. **5**, 129 (1984).
[32]W. L. Jorgensen, "OPLS all-atom parameters for organic molecules, ions, peptides and nucleic acids, July 2008," as provided by W. L. Jorgensen, Yale University during June 2009. These parameters are taken from those distributed with BOSS Version 4.8.

Downloaded from http://pubs.aip.org/aip/jcp/article-pdf/doi/10.1063/5.0106722/16552584/134901_1_online.pdf

Published under an exclusive license by AIP Publishing

[33]C. Gray and K. Gubbins, *Theory of Molecular Fluids. Volume 1: Fundamentals* (Clarendon Press, 1984).
[34]*CRC Handbook of Chemistry and Physics*, 102nd ed., edited by J. Rumble (CRC Press, London, England, 2021).
[35]J. A. Rackers, Z. Wang, C. Lu, M. L. Laury, L. Lagardère, M. J. Schnieders, J.-P. Piquemal, P. Ren, and J. W. Ponder, "Tinker 8: Software tools for molecular design," J. Chem. Theory Comput. **14**, 5273 (2018).
[36]G. Bussi and M. Parrinello, "Stochastic thermostats: Comparison of local and global schemes," Comput. Phys. Commun. **179**, 26 (2008).
[37]H. J. C. Berendsen, J. P. M. Postma, W. F. Van Gunsteren, A. Dinola, and J. R. Haak, "Molecular dynamics with coupling to an external bath," J. Chem. Phys. **81**, 3684 (1984).
[38]S. Toxvaerd and J. C. Dyre, "Communication: Shifted forces in molecular dynamics," J. Chem. Phys. **134**, 081102 (2011).
[39]D. Wolf, P. Keblinski, S. R. Phillpot, and J. Eggebrecht, "Exact method for the simulation of Coulombic systems by spherically truncated, pairwise r^{-1} summation," J. Chem. Phys. **110**, 8254 (1999).
[40]P. J. Steinbach and B. R. Brooks, "New spherical-cutoff methods for long-range forces in macromolecular simulation," J. Comput. Chem. **15**, 667 (1994).
[41]M. Lamichhane, K. E. Newman, and J. D. Gezelter, "Real space electrostatics for multipoles. II. comparisons with the Ewald sum," J. Chem. Phys. **141**, 134110 (2014).
[42]M. P. Allen and D. J. Tildesley, *Computer Simulation of Liquids* (Oxford University Press, 2017).
[43]J. Vieillard-Baron, "The equation of state of a system of hard spherocylinders," Mol. Phys. **28**, 809 (1974).
[44]S. Khodadadi and A. P. Sokolov, "Protein dynamics: From rattling in a cage to structural relaxation," Soft Matter **11**, 4984 (2015).
[45]R. Pastore, A. Coniglio, and M. Pica Ciamarra, "From cage-jump motion to macroscopic diffusion in supercooled liquids," Soft Matter **10**, 5724 (2014).
[46]C. H. Rycroft, "VORO++: A three-dimensional Voronoi cell library in C++," Chaos **19**, 041111 (2009).
[47]W. Mickel, S. C. Kapfer, G. E. Schröder-Turk, and K. Mecke, "Shortcomings of the bond orientational order parameters for the analysis of disordered particulate matter," J. Chem. Phys. **138**, 044501 (2013).
[48]W. Shen, J. Antonaglia, J. A. Anderson, M. Engel, G. Van Anders, and S. C. Glotzer, "Symmetries in hard polygon systems determine plastic colloidal crystal mesophases in two dimensions," Soft Matter **15**, 2571 (2019).
[49]M. P. Lettinga and E. Grelet, "Self-diffusion of rodlike viruses through smectic layers," Phys. Rev. Lett. **99**, 197802 (2007).
[50]G. S. Kottas, L. I. Clarke, D. Horinek, and J. Michl, "Artificial molecular rotors," Chem. Rev. **105**, 1281 (2005).
[51]J. Leisen, M. Werth, C. Boeffel, and H. W. Spiess, "Molecular dynamics at the glass transition: One dimensional and two dimensional nuclear magnetic resonance studies of a glass-forming discotic liquid crystal," J. Chem. Phys. **97**, 3749 (1992).
[52]I. Fischbach, T. Pakula, P. Minkin, A. Fechtenkötter, K. Müllen, H. W. Spiess, and K. Saalwächter, "Structure and dynamics in columnar discotic materials: A combined X-ray and solid-state NMR study of hexabenzocoronene derivatives," J. Phys. Chem. B **106**, 6408 (2002).
[53]F. Vaca Chávez, P. J. Sebastião, Y. Miyake, H. Monobe, and Y. Shimizu, "Dynamics of discotic fluoroalkylated triphenylene molecules studied by proton NMR relaxometry," J. Phys. Chem. B **116**, 2339 (2012).
[54]J. Timmermans, "Plastic crystals: A historical review," J. Phys. Chem. Solids **18**, 1–8 (1961).
[55]J. N. Sherwood, *The Plastically Crystalline State: Orientationally Disordered Crystals* (Wiley, 1979).
[56]I. M. Sokolov, "Models of anomalous diffusion in crowded environments," Soft Matter **8**, 9043 (2012).
[57]P. Polanowski and A. Sikorski, "Molecular transport in systems containing binding obstacles," Soft Matter **15**, 10045 (2019).
[58]P. Hopkins, A. Fortini, A. J. Archer, and M. Schmidt, "The van Hove distribution function for Brownian hard spheres: Dynamical test particle theory and computer simulations for bulk dynamics," J. Chem. Phys. **133**, 224505 (2010).
[59]L. Van Hove, "Correlations in space and time and Born approximation scattering in systems of interacting particles," Phys. Rev. **95**, 249 (1954).
[60]A. Cuetos, N. Morillo, and A. Patti, "Fickian yet non-Gaussian diffusion is not ubiquitous in soft matter," Phys. Rev. E **98**, 042129 (2018).
[61]S. Belli, A. Patti, R. van Roij, and M. Dijkstra, "Heterogeneous dynamics in columnar liquid crystals of parallel hard rods," J. Chem. Phys. **133**, 154514 (2010).
[62]N. Boden, R. J. Bushby, J. Clements, K. Donovan, B. Movaghar, and T. Kreouzis, "Charge dynamics and recombination kinetics in columnar discotic liquid crystals," Phys. Rev. B **58**, 3063 (1998).
[63]X. Shen, R. Y. Dong, N. Boden, R. J. Bushby, P. S. Martin, and A. Wood, "Orientational ordering and dynamics in the columnar phase of a discotic liquid crystal studied by deuteron NMR spectroscopy," J. Chem. Phys. **108**, 4324 (1998).

Downloaded from http://pubs.aip.org/aip/jcp/article-pdf/doi/10.1063/5.0106722/16552584/134901_1_online.pdf

Published under an exclusive license by AIP Publishing